Available online at www.sciencedirect.com
ScienceDirect
Journal of Power Sources 179 (2008) 763–769
JOURNAL OF POWER SOURCES
www.elsevier.com/locate/jpowsour

Electrical and dielectric properties of lithium manganate nanomaterials doped with rare-earth elements

Muhammad Javed Iqbal *, Zahoor Ahmad

Department of Chemistry, Quaid-i-Azam University, Islamabad 45320, Pakistan

Received 13 September 2007; accepted 29 December 2007
Available online 17 January 2008

Abstract

Substituted $LiR_xMn_{2-x}O_4$ ($R = La^{3+}$, Ce^{3+}, Pr^{3+} and $x = 0.00 - 0.20$) nanoparticles are prepared by the sol–gel method and the consequent changes in their lattice structure, dielectric and electrical parameters are determined by XRD, ED-XRF, SEM, LCR meter bridge and dc electrical resistivity measurements. Diffraction data show that the samples are single-phase spinel materials with crystallites sizes between 21 and 38 nm. The lattice parameter, cell volume and X-ray density are found to be affected by doping the Li-manganate with the rare-earth elements. The ED-XRF analysis confirms the stoichiometric composition of the synthesized samples and SEM reveals their morphology. Calculated values of the dielectric constant ($\acute{\varepsilon}$) and the dielectric loss ($\tan\delta$) decrease with the frequency of the applied field. This is attributed to Maxwell–Wagner polarization. Replacement of manganese by the rare-earth elements results in an improvement in the structural stability of the material, which is considered to be useful for enhancement of the cycleability of the compounds when used in lithium rechargeable batteries, and increases significantly the values of $\acute{\varepsilon}$ and $\tan\delta$ (except for Ce). Lithium manganate nanomaterials with high $\acute{\varepsilon}$ and low $\tan\delta$ may be attractive for application in memory storage devices.

Keywords: Lithium manganate; Nanomaterial; Electrical resistivity; Dielectric properties; Rare-earth element; Lithium rechargeable battery

1. Introduction

Nanocrystalline materials have shown significant promise in industry and technology [1]. This is mainly because their optical, electrical, mechanical, electronic and chemical properties are a function of their dimensions, which makes them superior in various applications compared with their bulk counterparts [2]. The use of nanocrystalline materials will lead to the miniaturization and exploitation of their unique properties. Recently, with the development of mobile communication and portable computers, there is an increasing requirement for advance energy-storage systems with high specific energy and power capacity [3]. The increased demand for lithium-ion battery applications such as hybrid electrical vehicles (HEVs) and electrical vehicles (EVs) has attracted much attention in search of low cost, safer and non-toxic cathode materials [4]. Lithium manganese oxide ($LiMn_2O_4$) is by far the most promising material for lithium rechargeable batteries. In general, for battery applications, $LiMn_2O_4$ powder possessing a single-phase, good homogeneity, uniform particle morphology with sub-micron size distribution and large surface area is desirable in order to achieve better electrode properties [5,6]. The intrinsic properties of ceramic materials are influenced by: (i) the shape, size, orientation, voids, inhomogeneities, etc. of the grains, (ii) the large percentage of their atoms in grain boundary environments and (iii) the interactions between grains [7].

In order to obtain pure crystalline, single, domain particles of lithium manganese oxide, different synthetic techniques such as sol–gel precipitation [8], the Pechini process [9], microemulsion [10,11] and electrochemical processes [12,13] have been developed. In this work, a citrate precursor method [14] has been adopted for the synthesis of lithium manganese oxide and its rare-earth element-doped derivatives. Because this method offers several advantages such as a high degree of homogeneity, a narrow particle-size distribution, a high surface area to volume ratio, good control of stoichiometry, lower calcination temperature and shorter processing time [15]. Iqbal and Zahoor [16] have reported the effect of annealing temperature on the struc-

* Corresponding author. Tel.: +92 51 90642143; fax: +92 51 90642241.
E-mail address: mjiqauchem@yahoo.com (M.J. Iqbal).

0378-7753/$ – see front matter © 2008 Elsevier B.V. All rights reserved.
doi:10.1016/j.jpowsour.2007.12.115

tural and electrical properties of $LiMn_2O_4$ doped with Cr, Fe, Co, Ni, Cu and Zn. Liu et al. [17] have studied the thermal, structural and electrochemical properties of Er-doped $LiMn_2O_4$. Zhengshun et al. [18] have investigated the electrochemical properties of $LiMn_2O_4$ in which Mn was partly replaced by Nd and Ce. To the best of authors' knowledge, the dielectric properties of lithium manganate nanomaterials have not been reported. These materials have high dielectric constants, low dielectric losses, and, therefore, they are extensively applicable in discrete and multilayer (MLC) capacitors, microwave telecommunications applications and low-loss substrates for microwave integrated circuits [19]. The high dielectric constant materials are also very significant in advanced microelectronics technologies such as dynamic random access memories (DRAM) [20].

The main purpose of the present work is to minimize the crystallite size, enhance the structural stability and dielectric properties of the lithium manganese oxide by substitution of rare-earth elements (La^{3+}, $Ce^{3+}$and Pr^{3+}). An attempt is made to evaluate the affect of the substituents on the electrical and dielectric properties of $LiMn_2O_4$.

2. Experimental

The materials used in the synthesis of $LiMn_2O_4$ and its derivatives doped with rare-earth elements were prepared from high-purity chemicals, namely: manganese acetate tetra hydrate (Merck, 99.9%), lithium nitrate (Fluka, 98.5%), citric acid (Sigma, 99.5%), lanthanum nitrate hexa hydrate (BDH, 98%), cerium nitrate hexa hydrate (Merck, 98.5%), praseodymium nitrate penta hydrate (Fluka, 99%), and ammonia solution (Aldrich, 33.0%).

The citric acid assisted sol–gel method [14] has been adopted to prepare nanosized lithium manganate and its derivatives doped with rare-earth elements for the present investigation. Aqueous solutions of manganese acetate, lithium nitrate and citric acid were mixed with mild stirring in a molar ratio of Li:Mn:citric acid = 1:2:3. The pH of the mixed solution was maintained at 7.0 using a pH meter and drop-wise addition of 2.0 M ammonia solution. In order to remove excess ammonia and water, the solution was heated on a hot plate at 80 °C for 4 h with vigorous stirring until a gel was formed. The metal-citrate gel was dried in an oven at 120 °C for 8 h to form the precursor. The dried sample was then sintered in air using a temperature-programmed tube furnace at a heating rate of 5 °C per min at 800 °C for 8 h.

The compound formation, phase purity and crystallinity of the prepared spinel materials were identified by powder XRD patterns recorded with a PANalytical 3040/60 X'Pert PRO X-ray diffractometer equipped with a Cu Kα radiation source of 45 kV and 40 mA. The procedure involved a step of 0.04° over a range of 10–80° and a scan speed of 1 s per step. The nominal compositions of the synthesized materials, i.e., $LiR_xMn_{2-x}O_4$ (R = La^{3+}, Ce^{3+}, Pr^{3+} and $x = 0.00$–0.20), were confirmed by means of ED-XRF spectrometry (Horiba MESA-500). The morphological features were analyzed through scanning electron microscopy (Hitachi S-3400N). The dc electrical resistivity was measured over a temperature range of 298 to 653 ± 5 K by the two-point probe method described elsewhere [21]. Dielectric measurements were performed at room temperature in a frequency range of 100 Hz to 1 MHz using an LCR meter bridge (Wayne Kerr LCR 4275).

3. Results and discussions

3.1. XRD analysis

XRD patterns of $LiR_xMn_{2-x}O_4$ (where R = La^{3+}, Ce^{3+}, $Pr^{3+}$and $x = 0.00 - 0.20$) are shown in Figs. 1–3. Well-defined sharp peaks with high crystallinity and perfect matching with the standard pattern of $LiMn_2O_4$ (JCPDS card 00-035-0782) are obtained for all the synthesized samples. The presence of peaks corresponding to the planes (1 1 1), (3 1 1), (2 2 2), (4 0 0), (3 3 1), (5 1 1), (4 4 0) and (5 3 1) ratifies the well-defined spinel structure without any impurity.

The lattice constant (a) of each sample is calculated from the *hkl* values of the diffraction peaks [22]. It can be seen from Table 1 that the value of the lattice constant for $LiMn_2O_4$ samples containing different concentrations of La^{3+}, $Ce^{3+}$and Pr^{3+} is in the range 8.19 to 8.25 ± 0.02 Å. These values are in concordance with the standard data for $LiMn_2O_4$ spinel material (a = 8.24 Å) given in JCPDS card 00-035-0782 [23]. Although the ionic radii of the doped La^{3+} (1.15 Å), Ce^{3+} (1.01 Å) and Pr^{3+} (1.09 Å) are larger than that of Mn^{3+} (0.66 Å) [24], it is clear from the data in Table 1 that the value of lattice constant decreases with increasing dopant concentration because the rare-earth elements doped in the octahedral sites have larger binding energy compared with the parent Mn^{3+} ion [25]. In addition, the rare-earth elements reduce the Mn^{3+} content, increase the average ionic valence of the Mn ion, constrain the possibility of Jahn-Teller distortion, and stabilize the cubic spinel structure of $LiMn_2O_4$ [17]. This stabilization enhances the cycling

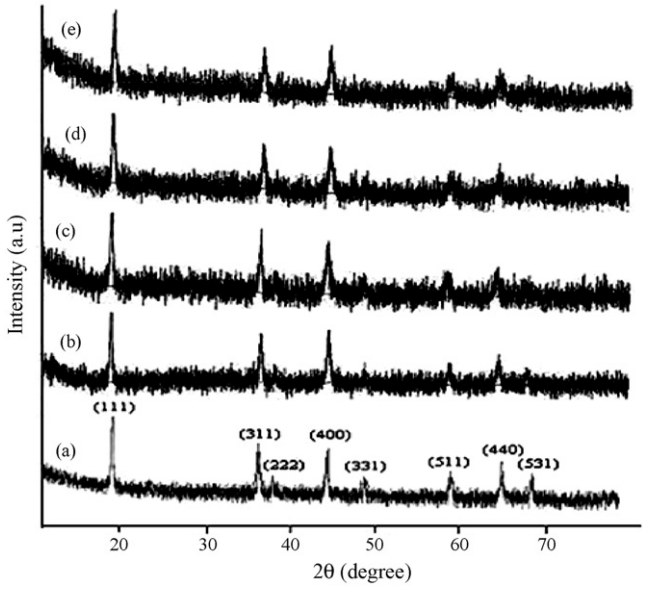

Fig. 1. Comparison of XRD patterns of $LiLa_xMn_{2-x}O_4$ samples where (a) $x = 0.00$, (b) $x = 0.04$, (c) $x = 0.08$, (d) $x = 0.12$, (e) $x = 0.16$ and (f) $x = 0.20$.

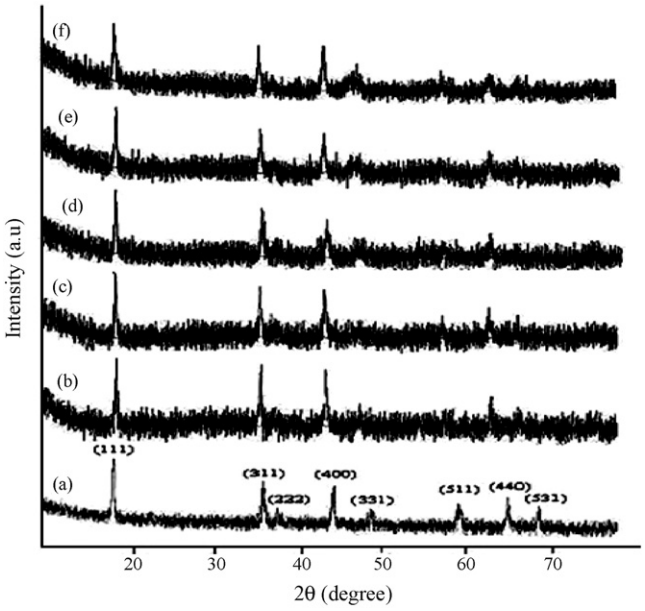

Fig. 2. Comparison of XRD patterns of $LiCe_xMn_{2-x}O_4$ samples where (a) $x = 0.00$, (b) $x = 0.04$, (c) $x = 0.08$, (d) $x = 0.12$, (e) $x = 0.16$ and (f) $x = 0.20$.

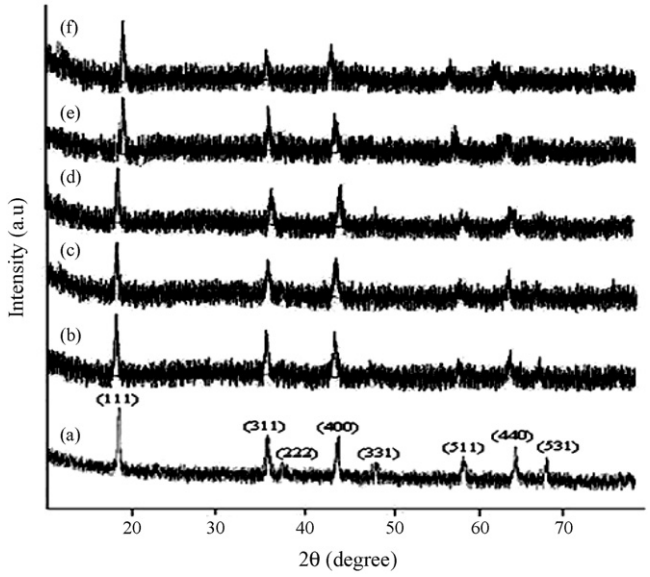

Fig. 3. Comparison of XRD patterns of $LiPr_xMn_{2-x}O_4$ samples where (a) $x = 0.00$, (b) $x = 0.04$, (c) $x = 0.08$, (d) $x = 0.12$, (e) $x = 0.16$ and (f) $x = 0.20$.

reversibility of lithium batteries [26,27]. The results are comparable with those evaluated by Liu et al. [17] and Zheng-shun et al. [18]. The above-mentioned improvement in the binding energy of $LiMn_2O_4$ structure as a result of the doping of La^{3+}, $Ce^{3+}$and Pr^{3+} is therefore considered to be useful. The cell volume ($V = a^3$) of the samples is also calculated and is found to vary in a similar manner to that of the lattice constant (Table 1).

The X-ray densities of the samples are calculated from the relationship: $d_x = ZM/N_A V_{cell}$ [28]. The value of X-ray density increases with increase in dopant concentration (Table 1). This may be due to the combined effect of two factors, namely, (i) larger molar mass of the rare-earth elements than that of manganese and (ii) the enhancement in the binding energy as discussed above.

The values of the crystallite size (D) of the synthesized samples are calculated by the well-known Scherrer formula [29], and are found in the range 21 to 38 ± 0.01 nm.

The expected theoretical stoichiometric molar quantities of Mn^{3+}, La^{3+}, Ce^{3+} and Pr^{3+} in the synthesized samples are comparable with the values calculated from ED-XRF data given in Table 2. The small error in the experimental (<2%) values may be due to the highly hygroscopic nature of the rare-earth element salts used for the preparation.

3.2. SEM analysis

It is well known that the surface morphology and particle-size distribution are also important determinants of the electrochemical performance of lithium secondary batteries. Therefore, the

Table 1
Comparison of lattice parameter (a), cell volume (V), crystallite size (D) and X-ray density (d_x) of $LiR_xMn_{2-x}O_4$ (R = La^{3+}, Ce^{3+}, Pr^{3+} and $x = 0.00 - 0.20$)

Samples	a (Å) ±0.01	V (Å^3) ±0.01	D (nm) ±0.02	d_x (g cm^{-3}) ±0.02
$LiMn_2O_4$	8.24	559.47	36.98	4.32
$LiLa_{0.04}Mn_{1.96}O_4$	8.22	555.41	27.20	4.41
$LiLa_{0.08}Mn_{1.92}O_4$	8.23	557.44	29.00	4.50
$LiLa_{0.12}Mn_{1.88}O_4$	8.21	553.38	20.80	4.58
$LiLa_{0.16}Mn_{1.84}O_4$	8.20	551.37	28.70	4.64
$LiLa_{0.20}Mn_{1.80}O_4$	8.19	549.35	26.93	4.75
$LiCe_{0.04}Mn_{1.96}O_4$	8.25	561.51	37.78	4.36
$LiCe_{0.08}Mn_{1.92}O_4$	8.24	559.47	31.97	4.46
$LiCe_{0.12}Mn_{1.88}O_4$	8.23	557.44	24.96	4.54
$LiCe_{0.16}Mn_{1.84}O_4$	8.22	555.41	27.84	4.60
$LiCe_{0.20}Mn_{1.80}O_4$	8.21	553.38	26.36	4.71
$LiPr_{0.04}Mn_{1.96}O_4$	8.24	559.47	25.65	4.40
$LiPr_{0.08}Mn_{1.92}O_4$	8.23	557.44	35.36	4.48
$LiPr_{0.12}Mn_{1.88}O_4$	8.22	555.41	24.34	4.59
$LiPr_{0.16}Mn_{1.84}O_4$	8.21	553.38	23.98	4.68
$LiPr_{0.20}Mn_{1.80}O_4$	8.20	551.36	24.80	4.77

Table 2
Comparison of the theoretical and observed weight, determined by ED-XRF, of elements, i.e., La, Ce, Pr and Mn in $LiLa_{0.04}Mn_{1.96}O_4$, $LiCe_{0.04}Mn_{1.96}O_4$, and $LiPr_{0.04}Mn_{1.96}O_4$ samples

Samples		Number of moles	Observed weight (g)	Theoretical weight (g)
$LiLa_{0.04}Mn_{1.96}O_4$	La	0.043	5.973	5.899
	Mn	1.950	107.129	107.100
$LiCe_{0.04}Mn_{1.96}O_4$	Ce	0.041	5.745	5.665
	Mn	1.952	107.239	107.179
$LiPr_{0.04}Mn_{1.96}O_4$	Pr	0.040	5.594	5.520
	Mn	1.965	107.953	107.899

morphology of the spinel $LiMn_2O_4$ powders and its derivatives obtained by annealing the precursor for 8 h at 800 °C have been examined by the scanning electron microscopy (SEM) (Fig. 4). It can be seen that all of the synthesized powders have a uniform porous morphology with a narrow size distribution. On the other hand, the extent of agglomeration in the lithium manganate samples is greater. The particle size of the samples is in the range 40–80 nm. The difference between the particle sizes calculated from the Scherrer formula and those measured by SEM analysis indicates agglomeration of nanometer-size particles. The porous morphology of lithium manganate sample is beneficial for the diffusion of the electrolyte into the interior of the particle [30], because large surface area enhances manganese dissolution. Thus the extraction–insertion of lithium becomes easier, so that the cycleability (charge–discharge process) of the Li–Mn–O cathode is improved.

3.3. Electrical resistivity measurements

The dc electrical resistivity of various samples has been measured as a function of temperature from 298 to 673 K. Resistivity decreases with increase in temperature, as shown in Fig. 5, which indicates semi-conducting behaviour. Fig. 6 shows a clear rela-

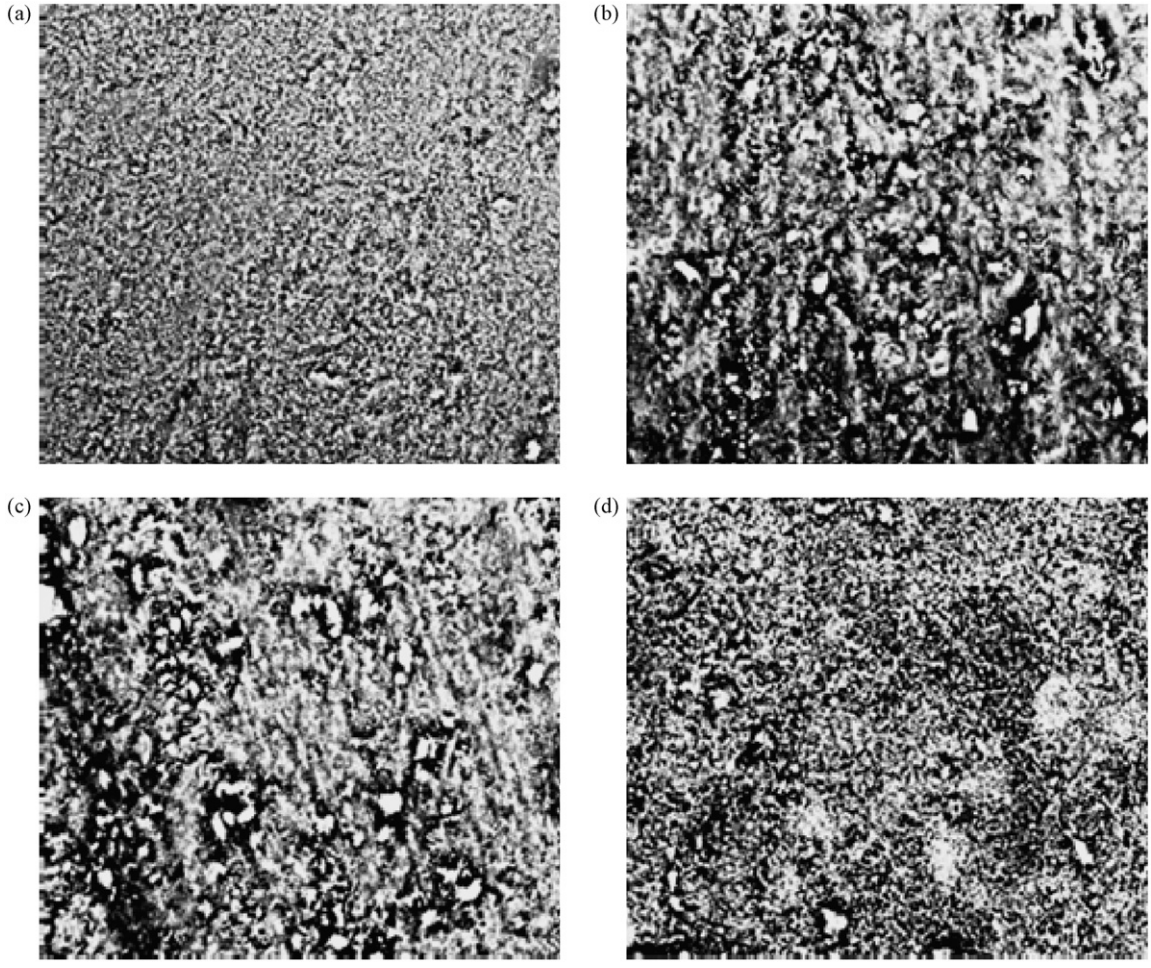

Fig. 4. Scanning electron micrographs of (a) $LiMn_2O_4$, (b) $LiLa_{0.12}Mn_{1.88}O_4$, (c) $LiCe_{0.12}Mn_{1.88}O_4$ and (d) $LiPr_{0.12}Mn_{1.88}O_4$.

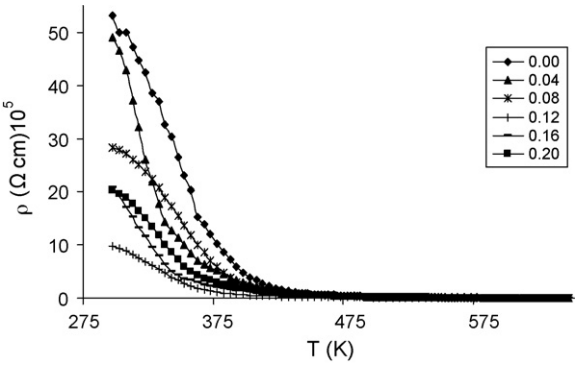

Fig. 5. Plot of dc electrical resistivity of $LiLa_xMn_{2-x}O_4$ ($x = 0.00 - 0.20$) samples vs. temperature.

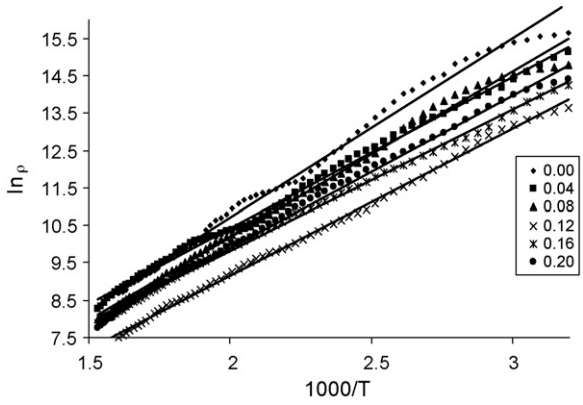

Fig. 7. Plot of ln ρ vs. $1/T$ for $LiLa_xMn_{2-x}O_4$ samples where $x = 0.00 - 0.20$.

tionship between electrical resistivity and the La^{3+}, $Ce^{3+}$and Pr^{3+} content, x, at a temperature of 298 ± 5 K. The resistivity of the substituted $LiMn_2O_4$ samples increases up to dopant concentration levels of $x \leq 0.16$ but decreases on further increase in concentration.

These observations can be explained on the basis of conduction in $LiMn_2O_4$ occurring via small-polaron hopping between Mn^{3+} and Mn^{4+}, i.e., unpaired electrons from the e_g orbitals of high-spin Mn^{3+} (d_4) hop to neighbouring low-spin Mn^{4+} (d_3) ions. Both the e_g orbitals of the metal ion lie on the same octahedral site so these are equivalent in energy and hopping is limited to orbitals of the same energy as has been described elsewhere [31].

Mn^{3+} acts as a small-polaron carrier in this system and a resulting decrease in their number would also lead to increase in resistivity of the substituted lithium manganate compounds [16]. The substitution of rare-earth ions tend to decrease the Mn^{3+} concentration at the octahedral sites and as a result the frequency of hopping of electron decreases. Exceeding the specific limit of the dopant concentration may cause the transfer of Mn^{3+} from the tetrahedral to the octahedral site and result in a decrease in resistivity. The loss in resistivity with temperature is mainly regarded as a consequence of the thermally activated mobility of the carriers (electrons or holes) [32].

The Arrhenius-type plot for the resistivity, ln ρ, of small-polaron conduction should be linear with temperature, $1/T$, in accordance with the relation, $\rho = \rho_o \exp(E_a/k_B T)$ [33], where ρ_o is a constant, E_a is the energy of activation, k_B is the Boltzmann constant. The plots of ln ρ versus $1/T$ for the samples containing the rare-earth elements as dopants are linear (Fig. 7). The Energy of activation of hopping (E_a) of the synthesized samples is calculated from the slope of the aforementioned plots and varies from 0.33 to 0.41 eV. Fig. 8 shows the dependence of E_a on La^{3+}, $Ce^{3+}$and Pr^{3+} content, x. The trend is comparable with the compositional variation of dc electrical resistivity (Fig. 6), as discussed above. The samples that have high resistivity also have high E_a, and vice versa.

3.4. Dielectric properties

To our knowledge, studies of the dielectric properties of lithium manganate nanoparticles have not been reported. Therefore, we measured the values of dielectric constant and dielectric loss of $LiMn_2O_4$ and its derivatives in a frequency range of 100 Hz to 1 MHz at room temperature. The results given in Figs. 9 and 10 show that the dielectric constant ($\acute{\varepsilon}$) and dielectric loss (tan δ) initially decrease rapidly with increase in frequency (f) and become constant at higher frequencies because the electron-exchange interaction (hopping) between the Mn^{3+} and

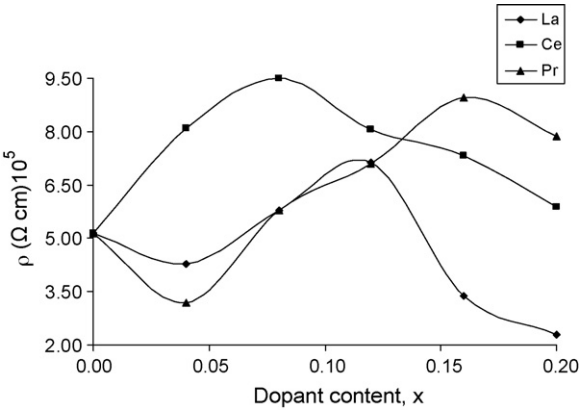

Fig. 6. Plot of dc electrical resistivity of $LiR_xMn_{2-x}O_4$ samples at 298 K vs. dopant ion content (x) where R = La^{+3}, Ce^{+3}, Pr^{+3} and $x = 0.00 - 0.20$.

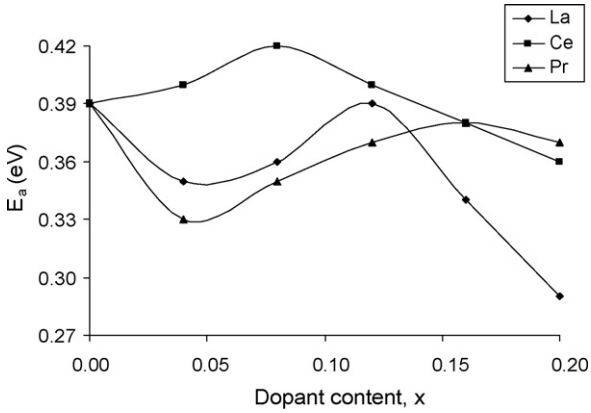

Fig. 8. Plot of activation energy of hoping (E_a) of $LiR_xMn_{2-x}O_4$ samples vs. dopant ion content where R = La^{+3}, Ce^{+3}, Pr^{+3} and $x = 0.00 - 0.20$.

Table 3
Comparison of dielectric constant ($\acute{\varepsilon}$) and dielectric loss ($\tan\delta$) of $LiR_xMn_{2-x}O_4$ (R = La^{3+}, Ce^{3+}, Pr^{3+} and $x = 0.00$ and 0.04)

Dielectric parameters	f (MHz)	$LiMn_2O_4$	$LiLa_{0.04}Mn_{1.96}O_4$	$LiCe_{0.04}Mn_{1.96}O_4$	$LiPr_{0.04}Mn_{1.96}O_4$
	0.001	3.80×10^6	7.00×10^6	9.70×10^3	2.18×10^7
$\acute{\varepsilon}$	0.1	830.41	903.53	478.50	1191.17
	1	124.00	127.00	62.00	240.00
	0.001	138.00	150.00	9.04	256.00
$\tan\delta$	0.1	2.27	3.19	0.94	4.26
	1	0.89	1.14	0.56	1.64

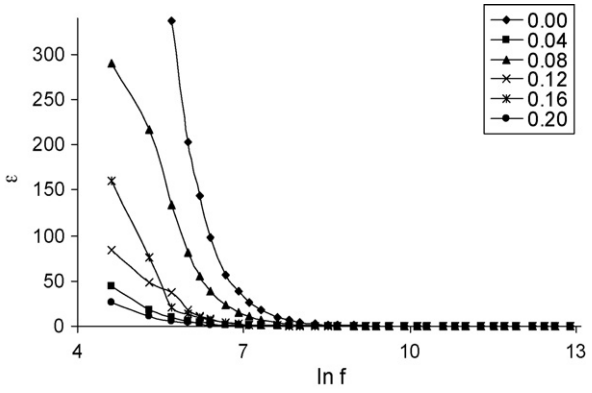

Fig. 9. Plot of dielectric constant of $LiLa_xMn_{2-x}O_4$ ($x = 0.00 - 0.20$) samples vs. ln f.

Mn^{4+} ions at the octahedral sites cannot follow the alternation of the applied ac electric field beyond a certain critical frequency. This behaviour may be due to the existence of interfacial polarization [34], which exists in a non-homogeneous layered structure of ceramic material as explained by Koops [35] on the basis of the Maxwell–Wagner model [36]. According to this model, the dielectric structure of a ceramic material is considered to be made up of two layers. The first layer consists of conducting grains and the second layer consists of poorly conducting grain boundaries. At lower frequencies, the grain boundaries are more active than the grains, while at higher frequencies only grains are active in electrical conduction. The polarization in manganates is via a conduction mechanism, i.e., electron-hopping between Mn^{3+} and Mn^{4+} ions at octahedral sites. This electron-hopping appears to be favourable at lower applied ac electric field frequencies; the dielectric constant has therefore a maximum value at lower frequencies. At high frequencies, however, the electron-exchange between Mn^{3+} and Mn^{4+} ions cannot follow the alternation of the applied ac electric field, hence $\acute{\varepsilon}$ and $\tan\delta$ fall to smaller values [37].

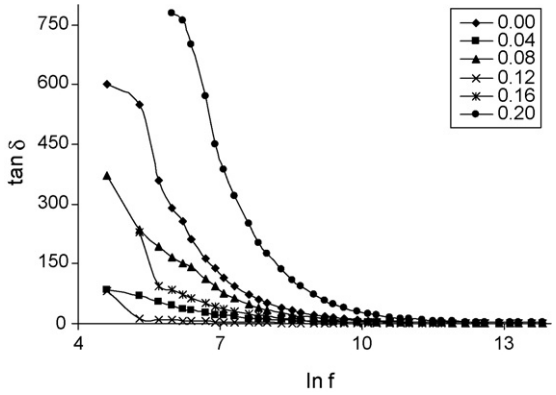

Fig. 10. Plot of dielectric loss of $LiLa_xMn_{2-x}O_4$ ($x = 0.00 - 0.20$) samples vs. ln f.

High dielectric constant materials are used in capacitors of dynamic random access memories (DRAM) for personal computers and workstations. The materials reported in the present study might also find potential application in temperature-compensating capacitors. The values of the dielectric constant at 1 kHz, 100 kHz and 1 MHz are listed in Table 3.

4. Conclusions

The sol–gel method is found to be suitable for the synthesis of nanosized $LiMn_2O_4$ spinel and its derivatives. X-ray diffraction data reveal the formation of single-phase spinel compounds and that the dopants preserve the cubic crystal structure of $LiMn_2O_4$. Further, the lattice constant and the X-ray density appear to be affected by the doped metal cations depending upon their nature. The uniform porous morphology of all the samples is confirmed by scanning electron microscopy. Studies of dc electrical resistivity show that a small-polaron hopping mechanism takes part in the conductivity of the samples investigated. The temperature-dependent dc electrical resistivity decreases with increase in temperature, and there-by validates the semiconductor nature of the samples. Samples with high resistivity also have high energy of activation, and vice versa. The dielectric constant and dielectric loss decrease with increasing frequency for all the samples. Both the dielectric constant and dielectric loss show frequency-dependent behaviour and ratify the effects that grains and grain boundaries have on conduction.

Acknowledgement

Financial support for this work by Higher Education Commission (HEC) of Pakistan is gratefully acknowledged.

References

[1] D.H. Chen, Y.Y. Chen, J. Colloid Interface Sci. 236 (2001) 41–46.
[2] G. Xiong, X. Wei, X. Yang, L. Lu, X. Wang, J. Mater. Sci. 35 (2000) 931–936.
[3] X. Wang, X. Chen, L. Gao, H. Zheng, M. Ji, T. Shen, Z. Zhang, J. Cryst. Growth 256 (2003) 123–127.
[4] S.S. Zhang, T.R. Jow, J. Power Sources 109 (2002) 172–177.

[5] M.M. Thackeray, W.I.F. David, P.G. Bruce, J.B. Goodenough, Mater. Res. Bull. 18 (1983) 461–466.
[6] J.M. Tarascon, E. Wang, F.K. Shokoohi, J. Electrochem. Soc. 38 (1991) 2859–2863.
[7] S. Kurien, S. Sebastian, J. Mathew, K.C. George, Indian J. Pure Appl. Phys. 42 (2004) 926–933.
[8] W. Liu, G.C. Farrington, F. Chaput, B. Dunn, J. Electrochem. Soc. 143 (1996) 879–884.
[9] W. Liu, K. Kowal, G.C. Farrington, J. Electrochem. Soc. 143 (1996) 3590–3596.
[10] K.T. Hwang, W.S. Um, H.S. Lee, J.K. Song, K.W. Chung, J. Power Sources 74 (1998) 169–174.
[11] C.H. Lu, S.W. Lin, J. Power Sources 93 (2001) 14–19.
[12] L.I. Hill, R. Portal, A. Verbaere, D. Guyomard, Electrochem. Solid State Lett. 4 (2001) A180–A185.
[13] L.I. Hill, R. Portal, G.L. Salle, A. Verbaere, D. Guyomard, Electrochem. Solid State Lett. 4 (2001) D1–D5.
[14] B.J. Hwang, R. Santhanam, D.G. Liu, J. Power Sources 97/98 (2001) 443–446.
[15] M.M. Amini, M. Mirzaee, N. Sepanj, Mater. Res. Bull. 42 (2007) 563–570.
[16] M.J. Iqbal, S. Zahoor, J. Power Sources 165 (2007) 393–397.
[17] H. Liu, L. Song, K. Zhang, Inorg. Mater. 41 (2005) 646–649.
[18] P. Zheng-shun, J. Yang, J. Zeng-yuan, Chin. Soc. Rare Earth 18 (2000) 115–119.
[19] L. Fang, Q. Yu, C. Hu, H. Zhang, Mater. Lett. 61 (2007) 4140–4143.
[20] G.L. Roberts, R.J. Cava, W.F. Peck, J. Am. Ceram. Soc. 58 (1997) 526–530.
[21] T. Abbas, M.U. Islam, M. Ashraf, Mod. Phys. Lett. B 9 (1995) 1419–1426.
[22] A.A. Sattar, Egypt. J. Sol. 27 (2004) 99–110.
[23] H.M. Wu, J.P. Tu, Y.F. Yuan, X.T. Chen, J.Y. Xiang, X.B. Zhao, G.S. Cao, J. Power Sources 161 (2006) 1260–1263.
[24] G.S. Rohrer, Structure and Bonding in Crystalline Materials, Cambridge University Press, UK, 2001, pp. 472–473.
[25] N. Hayashi, H. Ikuta, M. Wakihara, J. Electrochem. Soc. 146 (1999) 1351–1356.
[26] S.T. Myung, S. Komaba, N. Kumagai, J. Electrochem. Soc. 148 (2001) 482–488.
[27] K. Kanamura, K. Dokko, T. Kaizawa, J. Electrochem. Soc. 152 (2005) A391–A395.
[28] Y.S. Hong, C.M. Ho, H.Y. Hsu, C.T. Liu, J. Magn. Magn. Mater. 279 (2004) 401–406.
[29] M.J. Iqbal, S. Farooq, Mater. Sci. Eng. B 136 (2007) 140–147.
[30] X.C. Tang, L.P. He, Z.Z. Chen, D.Z. Jia, Chin. J. Inorg. Chem. 18 (2002) 591–594.
[31] I. Vitioo, PhD Thesis, Synthesis, structure, conductivity and electrode properties for some double disulphates, silicates and lithium manganese oxide, University of Latvia, Latvia, 1999.
[32] N. Iftimie, E. Rezlescu, P.D. Popa, N. Rezlescu, J. Optoelectron. Adv. Mater. 7 (2005) 911–914.
[33] R. Raman, V.R.K. Murthy, B. Viswanathan, J. Appl. Phys. 69 (1991) 4053–4055.
[34] M.A. Abdullah, A.N. Yusoff, J. Alloys Compd. 233 (1996) 129–133.
[35] C.G. Koops, Phys. Rev. 83 (1951) 121–127.
[36] K.W. Wagner, Ann. Phys. 40 (1913) 817–825.
[37] S. Angappan, L.J. Berchmans, C.O. Augustin, Mater. Lett. 58 (2004) 2283–2289.